Influence of ZnS and MgO Shell on the Photoluminescence Properties of ZnO Core/Shell Nanowires

ARTICLE *in* THE JOURNAL OF PHYSICAL CHEMISTRY C · DECEMBER 2009

Impact Factor: 4.77 · DOI: 10.1021/jp909176p

4 AUTHORS, INCLUDING:

Haowei Peng
National Renewable Energy Laboratory
31 PUBLICATIONS **633** CITATIONS

Influence of ZnS and MgO Shell on the Photoluminescence Properties of ZnO Core/Shell Nanowires

X. Q. Meng, Haowei Peng, Y. Q. Gai, and Jingbo Li*

State Key Laboratory for Superlattices and Microstructures, Institute of Semiconductors, Chinese Academy of Sciences, P.O. Box 912, Beijing 100083, P. R. of China

Received: September 23, 2009; Revised Manuscript Received: November 24, 2009

By sequential growth of the core and shell of different materials, ZnO/ZnS and ZnO/MgO core/shell nanowire arrays are fabricated. Photoluminescence properties of these samples with different shell thicknesses are studied in detail. The results indicate that the ZnS shell thickness as a function of treatment time will noticeably change the photoluminescence intensity of the ZnO nanowires, whereas the MgO shell will not change the photoluminescence intensity any more after it saturates the surface dangling bonds of ZnO core. Large-scale first-principles calculations indicate that, unlike the ZnO/MgO core/shell nanowires, the electrons and holes of which are both confined in the core of the nanowires (type-I heterostructures), the ZnO/ZnS core/shell nanowires are type-II heterostructures, the electrons and holes of which are respectively confined in the core and the shell; as a result, the separation of electrons and holes in the ZnO/ZnS core/shell nanowires will reduce the spatial overlap between them, leading to the decrease of the photoluminescence intensity in this system. The experimental observations are in good agreement with first-principles calculations (PACS: 62.23.Hj, 71.55.Gs, 73.40.Lq, 74.25.Gz, 73.43.Cd).

1. Introduction

By combining the properties of both semiconductor and nanostructures, one-dimensional semiconductor nanowires are perhaps the most prospective materials for nanoscale sensors, light emitting diodes, solar cells, and so forth.[1,2] However, the defects such as surface states and band-gap mismatch in semiconductor nanowires will limit their application for the optoelectronic and photoelectronic devices. By depositing a layer of shell on the nanowires to fabricate core/shell nanowires, the surface states of the core will be modified, the band gap of the core material can be tailored, and as a result, the properties including photoluminescence (PL) of the core will be improved.[3] Among the various semiconductor nanostructures, ZnO is always a predominate one owning to its large band gap (3.3 eV at room temperature) and excellent optoelectronic properties.[4] To enhance the PL properties of ZnO nanowires, ZnO core/shell structures have also been extensively studied.[5−11] The shell material plays a key role in the enhancement of PL properties. However, there is little knowledge about selecting suitable shell material. For example, ZnS and MgO are usually candidates as shell materials,[10,12] but there is no good reason for the selection. In this study, through first-principles band-structure and charge-density calculations, we find that the ZnO/MgO core/shell nanowire is a type-I heterostructure, whereas the ZnO/ZnS core/shell nanowire is a type-II heterostructure. As a result, we presume that there will be a large difference on PL properties of the two types of core/shell structures. Therefore, we fabricate the ZnO/ZnS and ZnO/MgO core/shell nanowire arrays by a two-step method. The changes of the optical properties of these core/shell nanowires as the shell thickness increases are investigated, and the origins of these changes are also discussed. The different tendencies of the optical properties of the ZnO/ZnS and ZnO/MgO core/shell nanowires are due to their different electronic structures. The experimental results fit well with theoretical calculations (PACS: 62.23.Hj, 71.55.Gs, 73.40.Lq, 74.25.Gz, 73.43.Cd).

2. Experimental Details

2.1. Preparation of ZnO/ZnS Core/Shell Nanowire Arrays. The samples are prepared by a two-step method. Well-aligned ZnO nanowire arrays are first grown in a traditional horizontal furnace by a simple vapor-phase transport process at 600 °C, similar with that reported earlier.[13] The as-synthesized sample is then cut into pieces for the following ZnS layer growth. The preparation of ZnS shell is carried out in two steps.[14] First, ZnO samples are immersed in Na_2S solution for a certain time. Then, the samples are immersed in Zn $(NO_3)_2$ solution for the same time as that for the Na_2S solution. The reaction time in each solution is 30, 60, 120, and 180 min. After being taken out of the solution and washed with deionized water, the samples are dried at 50 °C under vacuum conditions. The as-synthesized sample and the samples treated for 30, 60, 120, and 180 min are labeled as sample A, B, C, D, and E, respectively.

2.2. Preparation of ZnO/MgO Nanowire Arrays. The ZnO nanowires are synthesized as mentioned above. The fabrication of MgO shell is carried out by a chemical bath reaction. The ZnO samples are submerged in a 10 mM solution of Mg $(NO_3)_2$ mixed with 20 mM of NaOH at 60 °C. Note that the PH value is crucial during the reaction (too large PH results in the total erosion of ZnO); here, we adjust the PH value to 10−11 by a series of experiments. The reaction times are 30, 60, and 120 min. After being taken out of the solution and washed with deionized water, the samples are dried at 50 °C under air conditions. The as-synthesized sample and samples treated for 30, 60, and 120 min are labeled as sample A_1, B_1, C_1, and D_1, respectively.

2.3. Method of Calculations. The first-principles electronic-structure calculations are performed with the local density approximation (LDA) based on the density functional theory

* Corresponding author. E-mail: jbli@semi.ac.cn.

10.1021/jp909176p
Published on Web 12/30/2009

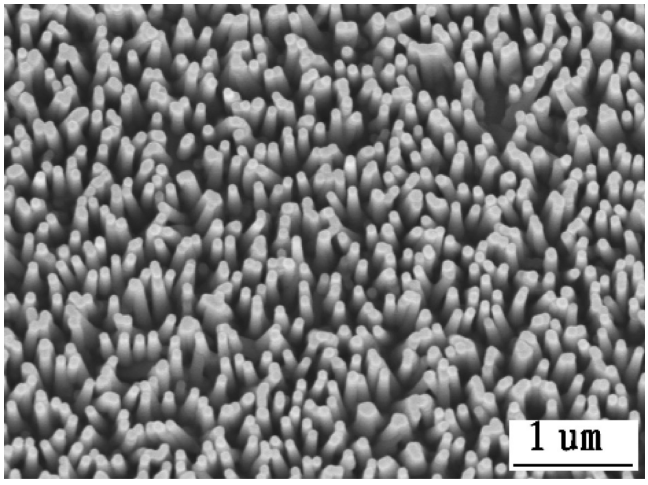

Figure 1. FESEM image of the as-synthesized ZnO nanowire arrays synthesized at 600 °C.

(DFT), as implemented in the Vienna ab initio simulation package (VASP).[15] The projector augmented wave method (PAW) is chosen to represent the ionic potentials.[16] In all the calculations, the convergence of the total energy with respect to the plane-wave bases kinetic-energy cutoff, and k-sampling is checked to be within 0.001 eV; all structures are relaxed until the Hellmann−Feynman force is less than 0.05 eV/Å. The Monkhorst−Pack method is used to sample the Brillouin zone.[17] The nanowires are built on the basis of the hexagonal WZ structure of ZnO, and the surface dangling bonds are fully passivated with pseudohydrogenatons (pseudo-H).[18,19] Specifically, the surface Zn of Mg dangling bonds are terminated with pseudo-H atoms with a nuclear charge of 1.5 e, and the surface O and S dangling bonds are terminated with pseudo-H atoms with a nuclear charge of 0.5 e. The number of atoms in the calculations is 400.

2.4. Characterization. Field-emission scanning electron microscopy (FESEM) images are acquired on a Hitachi S-4800 microscope instrument by using an accelerating voltage of 10 kV. High-resolution transmission electron microscopy (HRTEM) observations are carried out on a JEM-2010 microscope instrument by using an accelerating voltage of 200 kV. Steady-state PL spectra are recorded by using a Princeton sp2500 spectrometer that utilized a 325 nm He−Cd laser line of 30 mW. All the measurements are performed at room temperature under the same conditions; the reproducibility of the samples is confirmed by measuring several points for the same sample.

3. Results and Discussion

Figure 1 shows the FESEM image of the as-synthesized ZnO nanowire arrays. The image indicates that the nanowires are well aligned with a length of about 1 μm and a diameter of about 100 nm. Clear hexagonal shape and smooth surface reveal the high quality of the nanowires. After treatment with shell layers, the morphologies of the nanowires remain nearly the same as those of the as-synthesized one from the FESEM observations.[14] To further verify the morphological characteristics of the core/shell systems, HRTEM observation is introduced. The typical HRTEM images of sample C and B_1 are depicted schematically in the right part of Figure 2. For both samples, clear interface of the core/shell structures is observed. The thickness of the shell in sample C is about 8 nm (as shown in Figure 2a,b), whereas in sample B_1, it is about 10 nm (as shown in Figure 2c,d). Single-crystallized ZnO grows along the *c* axis with an interplanar distance of 0.52 nm, whereas polycrystallized hexagonal ZnS and cubic MgO grow along the *a* axis with an interplanar distance of 0.382 and 0.42 nm, respectively. More information can be obtained in the Supporting Information.

The evolution of the PL properties of the core/shell structures, as the ZnS treatment time increases from 0 to 180 min, are shown in Figure 3a. For sample A (ZnS treatment time of 0 min), a strong UV emission located at 3.218 eV and a weak visible emission are observed, which match the typical PL spectrum of ZnO. The UV emission is attributed to the band-gap emission of ZnO, and the visible emission originates from surface states or oxygen vacancies.[20,21] After modification by ZnS shells, both intensity and energy position of the emission change. For sample B, the intensity of the band-gap emission increases with a peak red-shift of about 9 meV, and the visible emission disappears. The band-gap emission increases remarkably with another red-shift of 9 meV for sample C; a similar shift in ZnO:S systems has been observed.[14,22,23] However, the intensity of the band-gap emission in sample E begins to decrease from that of sample D to only about a quarter of that of sample A. The evolution in intensity of the band-gap emission with increasing ZnS treatment time is shown in the insert of Figure 3a. Meanwhile, from sample D to sample E, the band-gap emission peak slowly blue-shifts back. For the ZnO/MgO core/shell nanowires with a 30 min treatment, the disappearance of the visible emission and the noticeable increase in intensity of the band-gap emission are also found. However, the intensity does not increase any more, even in sample D_1, as shown in Figure 3b. The evolution in intensity of the PL band-gap emission with increasing MgO treatment time is shown in the insert of Figure 3b. From sample B_1 to sample D_1, the band-gap emissions show a blue-shift of about 10 meV compared with that of sample A_1.

The treatment of ZnO with ZnS and MgO is a soft process. The thickness of ZnS and MgO shells increases with the increase of treatment time as demonstrated by HRTEM observations. At the beginning (from sample A to sample C for ZnO/ZnS systems and from sample A_1 to sample B_1 for ZnO/MgO systems), the PL intensity of both kinds of core/shell nanowires increases, indicating that the ZnS and MgO capping process greatly reduces the number of surface states. When ZnO is treated with ZnS for short times, ZnS slowly reacts with ZnO, part of the S atoms binds with the surface atoms of ZnO and saturates the surface dangling bonds, and the residual S atoms bind with Zn atoms in the following Zn $(NO_3)_2$ solution, forming ZnS. Because the ZnS layer covered on the surface of ZnO is thin, the whole electronic structure of the systems does not change too much. However, these thin shells are thick enough to terminate most of the dangling bonds on the surface of the ZnO nanowire core and will remove the surface states which act as career traps, leading to the drastic increase of the PL peak intensity, as shown in Figure 3a. At the same time, the visible emission disappears as the result of the elimination of surface states. For ZnO/MgO systems, the treatment method with MgO is different from that with ZnS. Two possible reactions occur at the first stage. One is that O ions saturate the surface states or oxygen vacancies of ZnO; then, Mg ions bind on the surface of ZnO, forming a thin layer. Another possible reaction is that the Mg−O complex first forms and then covers the surface of ZnO, and the bonded Mg−O complexes passivate the surface states of ZnO core. The two possible reactions lead to the increase of PL intensity. From sample D to sample E for ZnO/ZnS systems and from sample C_1 to sample D_1 for ZnO/

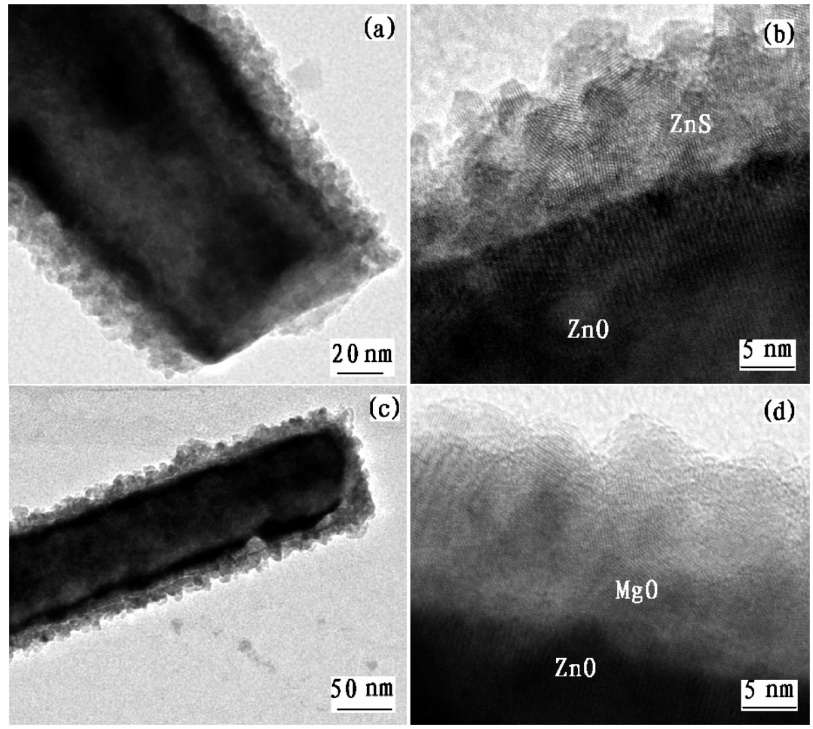

Figure 2. TEM and corresponding HRTEM images of (a) and (b) sample C and (c) and (d) sample B_1.

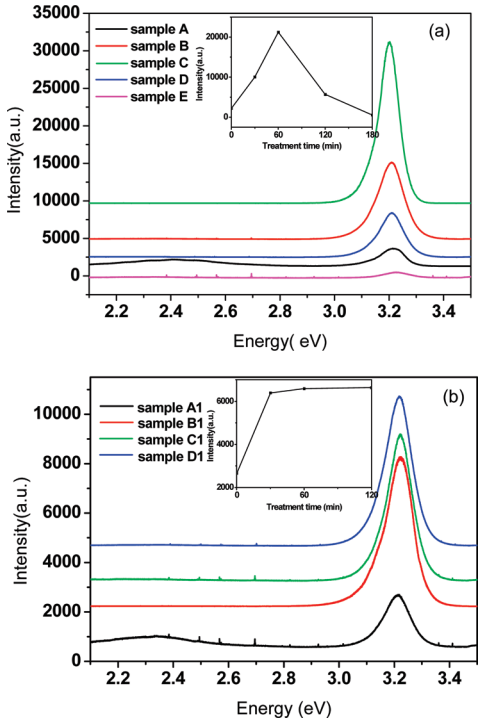

Figure 3. (a) PL properties of ZnO/ZnS core/shell structure with different ZnS shell treatment times and (b) PL properties of ZnO/MgO core/shell structure with different MgO shell treatment times. The insert is the PL energy position of the band-gap emission as a function of ZnS treatment time.

MgO systems, the PL properties of both kinds of systems show totally different trends. At this time, the shells are thick enough, and the differences can be attributed to their different electronic structures. According to the band alignment of the two components, the core/shell structures are typically classified into two types, type-I (the conduction band minimum (CBM) of the shell is of higher energy than that of the core, and the valence band maximum (VBM) of the shell is of lower energy than that of the core, which provides the lowest energy states for both electrons and holes) and type-II (both the valence and conduction bands in the core are lower (or higher) than that in the shell; therefore, the energy gradient existing at the interfaces tends to spatially separate electrons and holes on different sides of the heterojunction).[18,24,25] In type-I core/shell systems, the nanoscale exciton is confined to the core material, and the purpose of the shell is to passivate surface trap states and to protect the exciton from exposure to environmental factor.[26] In type-II core/shell systems, the electrons are confined in the core,

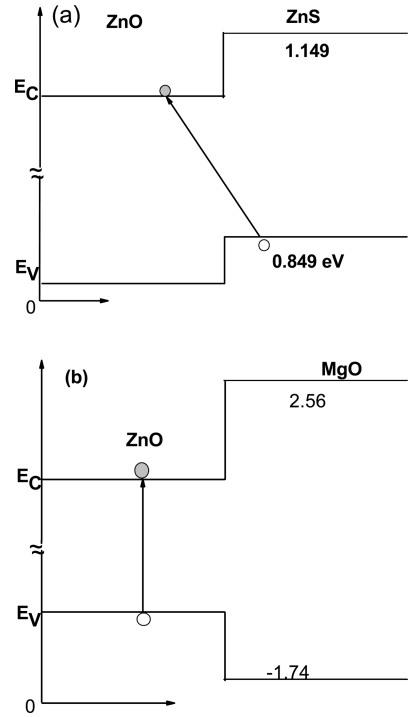

Figure 4. Schematic plots of the calculated band alignments of (a) ZnO/ZnS and (b) ZnO/MgO systems.

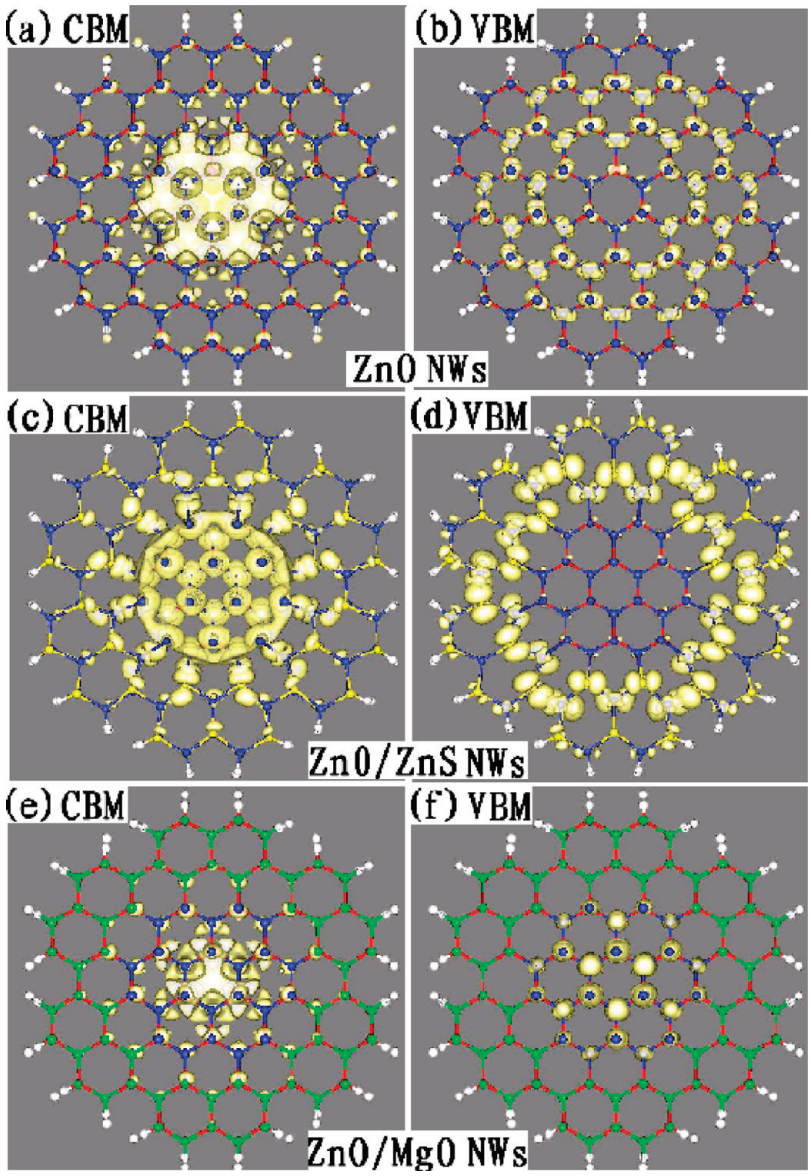

Figure 5. Contour plots of the charge densities of CBM and VBM states at point of (a) and (b) ZnO nanowires, (c) and (d) ZnO/ZnS core/shell nanowires, and (e) and (f) ZnO/MgO core/shell nanowires.

and the holes are located in the shell, which leads the core/shell systems to have many novel properties; for example, when comparing with either material in isolation, the emission spectrum shifts to lower energies, and the band-gap emission is quenched because of the spatial separation of electrons and holes.[27−29] (In our type-II core/shell systems, we mainly observed that the band-gap emission decreases.) In both types, the shell has a larger effect on the VBM states, whereas it only slightly modifies the CBM states of the core.[29] From the calculated band alignment of ZnO/ZnS and ZnO/MgO 2D superlattice, shown in Figure 4a,b, we can find that the ZnO/ZnS system has a type-II band aligment, whereas the ZnO/MgO system has a type-I band alignment. Wave-function squares of the CBM and VBM states of the ZnO nanowire and ZnO/ZnS and of the ZnO/MgO core/shell nanowires are also calculated. As shown in Figure 5c,d, the CBM states of the ZnO/ZnS core/shell nanowires are mainly distributed in the core section, whereas the VBM states are mainly in the shell section. Compared with the ZnO nanowire (Figure 5a,b), the overlap between the CBM and VBM states is mostly swept out; at this time, these structures absorb light across the UV spectrum, then separate electrons and holes across their type-II interface. The reduction in spatial overlap between electrons and holes results in the decrease of the PL intensity in the ZnO/ZnS systems.[29,30] Although in the ZnO/MgO systems, it is unusual for their special charge arrangement properties, the type-I band alignment provides a potential well for both the electrons and holes. The CBM and VBM states of the ZnO/MgO nanowire are confined in the core section, as shown in Figure 5e,f. The successful passivation of the surface states or oxygen vacancies of the ZnO nanowires can noticeably enhance the PL intensity. But a further increase of MgO thickness could not change the PL properties of the ZnO more.

To account for the energy shift of the PL peaks for the ZnO/ZnS systems, we need to consider the effects of crystal mismatch and reconstruction of the core/shell interface between the core and shell components. For ZnO/ZnS systems, because the crystal lattice constants of ZnS are larger than those of ZnO, the crystal lattice of ZnO core will expand to match with that of ZnS,[31] which results in a surface tensile strain. The red-shift of the PL band-gap emission in ZnO/ZnS system at the beginning is caused by such a strain, similarly to what happens in the CdSe/

ZnS systems.[31] When the ZnS layer gets thicker, two complete parts of ZnO and ZnS are formed, and the PL band-gap emission blue-shifts back from sample D to sample E, correspondingly. For the case of ZnO/MgO systems, the above-mentioned two possible reactions cause MgO to bind on the ZnO core, and the later reaction is probably the dominating one. Because the band gap of MgO is much larger than that of ZnO, the observed blue shift of the band-gap emission is considered as a combined effect of ZnO and MgO.

4. Conclusions

In summary, two types of core/shell structures of ZnO/ZnS and ZnO/MgO are successfully synthesized. The effects of the shell thickness on the PL properties are studied in detail. The optical properties of the two kinds of core/shell structures have different dependence on the shell thickness on the basis of their respective band alignment. The ZnO/ZnS samples have a type-II band alignment, the electrons of which are localized in the core and the holes of which are localized in the shell, which induces the separation of electrons and holes in the ZnO/ZnS core/shell nanowires and the reduction of the spatial overlap between them, causing the decrease of the PL intensity in this system. The ZnO/MgO samples have a type-I band alignment, the electrons and most holes of which are confined in the core. The observed results are well supported by the theoretical calculations.

Acknowledgment. J.L. gratefully acknowledges financial support from the One-Hundred Talent Plan of the Chinese Academy of Sciences and National Science Fund for Distinguished Young Scholar (Grant no. 60925016). This work is supported by the National High Technology Research and Development program of China under Contract no. 2009AA034101 and the Postdoctoral Foundation under Contract no. O9T1050000.

Supporting Information Available: This material is available free of charge via the Internet at http://pubs.acs.org.

References and Notes

(1) Dayeh, S. A.; Soci, C.; Yu, P. K. L.; Yu, E. T.; Wang, D. *J. Vac. Sci. Technol. B* **2007**, *25*, 1432.
(2) Reiss, A. P.; Protière, M.; Li, L. *Small* **2009**, *5*, 154.
(3) Wang, R. C.; Lin, H. Y. *Appl. Phys. A: Mater. Sci. Process.* **2009**, *95*, 813.
(4) Song, J. H.; Wang, X. D.; Riedo, E.; Wang, Z. L. *Nano. Lett.* **2005**, *5*, 1954.
(5) Richters, J. P.; Voss, T.; Kim, D. S.; Scholz, R.; Zacharias, M. *Nanotechnology* **2008**, *19*, 305202.
(6) Yu, L.; Yu, X. F.; Qiu, Y. F.; Chen, Y. J.; Yang, S. H. *Chem. Phys. Lett.* **2008**, *465*, 272.
(7) Han, S.; Zhang, D. H.; Zhou, C. W. *Appl. Phys. Lett.* **2006**, *88*, 133109.
(8) Qiu, M. X.; Ye, Z. Z.; He, H. P.; Zhang, Y. Z.; Tang, H. P.; Gu, X. Q.; Zhu, L. P.; Zhao, B. H.; Huang, J. Y.; Lu, J. G. *J. Phys. D: Appl. Phys.* **2008**, *41*, 85109.
(9) Yin, L. W.; Li, M. S.; Bando, Y.; Golberg, D.; Yuan, X. L.; Sekiguchi, T. *Adv. Funct. Mater.* **2007**, *17*, 270.
(10) Li, F.; Jiang, Y.; Hu, L.; Liu, L. Y.; Li, Z.; Huang, X. T. *J. Alloys Compd.* **2009**, *474*, 531.
(11) Ahn, C. H.; Mohanta, S. K.; Kong, B. H.; Cho, H. K. *J. Phys. D: Appl. Phys.* **2009**, *42*, 115106.
(12) Plank, N. V.; Snaith, H. J.; Ducati, C.; Bendall, J. S.; Mende, L. S.; Welland, M. E. *Nanotechnology* **2008**, *19*, 465603.
(13) Meng, X. Q.; Shen, D. Z.; Zhang, J. Y.; Zhao, D. X.; Lu, Y. M.; Dong, L.; Zhang, Z. Z.; Liu, Y. C.; Fan, X. W. *Solid State Commun.* **2005**, *135*, 179.
(14) Li, J. H.; Zhao, D. X.; Meng, X. Q.; Zhang, Z. Z.; Zhang, J. Y.; Shen, D. Z.; Lu, Y. M.; Fan, X. W. *J. Phys. Chem. B* **2006**, *110*, 14685.
(15) Kresse, G.; Joubert, D. *Mater. Sci.* **1996**, *6*, 15.
(16) Kresse, G.; Joubert, D. *Phys. Rev. B* **1999**, *59*, 1758.
(17) Monkhorst, H. J.; Pack, J. D. *Phys. Rev. B* **1976**, *13*, 5188.
(18) Li, J.; Wang, L. W. *Chem. Mater.* **2004**, *16*, 4012.
(19) Li, J.; Wang, L. W. *Phys. Rev. B* **1994**, *72*, 125325.
(20) Vanheusden, K.; Warren, W. L.; Sesger, C. H.; Tallant, D. R.; Voigt, J. A. B.; Gnage, E. *J. Appl. Phys.* **1996**, *79*, 7983.
(21) Yao, B. D.; Chan, Y. F.; Wang, N. *Appl. Phys. Lett.* **2002**, *8*, 757.
(22) Shen, G. Z.; Cho, J. H.; Yoo, J. K.; Yi, G. C.; Lee, C. J. *J. Phys. Chem. B* **2005**, *109*, 5491.
(23) Bae, S. Y.; Seo, H. W.; Park, J. H. *J. Phys. Chem. B* **2004**, *108*, 5206.
(24) Kim, S.; Fisher, B.; Eiser, H. J.; Bawendi, M. *J. Am. Chem. Soc.* **2003**, *125*, 11466.
(25) Kumar, S.; Jones, M.; Lo, S. S.; Scholes, G. D. *Small* **2007**, *3*, 1633.
(26) Ivanov, S. A.; Piryatinski, A.; Nanda, J.; Tretaik, S.; Zavadil, K. R.; Wallace, W. O.; Werder, D.; Klimov, V. I. *J. Am. Chem. Soc.* **2007**, *129*, 11708.
(27) Zhong, H. Z.; Scholes, G. D. *J. Am. Chem. Soc.* **2009**, *131*, 9170.
(28) He, J.; Lo, S. S.; Kim, J.; Scholes, G. D. *Nano. Lett.* **2008**, *8*, 4007.
(29) Milliron, D. J.; Hughes, S. M.; Cui, Y.; Manna, L.; Li, J. B.; Wang, L. W.; Alivisatos, A. P. *Nature* **2004**, *430*, 190.
(30) Kim, J.; Wong, C. Y.; Scholes, G. D. *Acc. Chem. Res.* **2008**, *42*, 1037.
(31) Baranov, A. V.; Rakovich, Y. P.; Donegan, J. F.; Perova, T. S.; Moore, R. A.; Talapin, D. V.; Rogach, A. L.; Masumoto, Y.; Nabiev, I. *Phys. Rev. B* **2003**, *68*, 165306.

JP909176P